Engineering 28 (2023) 117–129

Contents lists available at ScienceDirect

Engineering

journal homepage: www.elsevier.com/locate/eng

Research
Air Pollution Control—Article

Spatial and Temporal Variations in the Atmospheric Age Distribution of Primary and Secondary Inorganic Aerosols in China

Xiaodong Xie [a], Qi Ying [b], Hongliang Zhang [c], Jianlin Hu [a,*]

[a] Jiangsu Key Laboratory of Atmospheric Environment Monitoring and Pollution Control, Collaborative Innovation Center of Atmospheric Environment and Equipment Technology, Nanjing University of Information Science & Technology, Nanjing 210044, China
[b] Zachry Department of Civil Engineering, Texas A&M University, College Station, TX 77843, USA
[c] Department of Environmental Science and Engineering, Fudan University, Shanghai 200438, China

ARTICLE INFO

Article history:
Received 22 September 2021
Revised 6 December 2021
Accepted 23 March 2022
Available online 21 April 2022

Keywords:
Atmospheric age
$PM_{2.5}$
CMAQ model
Control strategy

ABSTRACT

The aging timescale of particles is a key parameter in determining their impacts on air quality, human health, and climate. In this study, a one-year simulation of the age distributions of the primary and secondary inorganic fine particulate matter ($PM_{2.5}$) components was conducted over China using an age-resolved Community Multiscale Air Quality (CMAQ) model. The results indicate that primary $PM_{2.5}$ (PPM) and ammonium mainly originate from fresh local emissions, with approximately 60%–80% concentrated in 0–24 h age bins in most of China throughout the year. The average age is about 15–25 h in most regions in summer, but increases to 40–50 h in southern region of China and the Sichuan Basin (SCB) in winter. Sulfate is more aged than PPM, indicating an enhanced contribution from regional transport. Aged sulfate with atmospheric age > 48 h account for 30%–50% of total sulfate in most regions and seasons, and the concentrations in the > 96 h age bin can reach up to 15 $\mu g \cdot m^{-3}$ in SCB during winter. Dramatic seasonal variations occur in the Yangtze River Delta, Pearl River Delta, and SCB, with highest average age of 60–70 h in winter and lowest of 40–45 h in summer. The average age of nitrate is 20–30 h in summer and increases to 40–50 h in winter. The enhanced deposition rate of nitric acid vapor combined with the faster chemical reaction rate of nitrogen oxides leads to a lower atmospheric age in summer. Additionally, on pollution days, the contributions of old age bins (> 24 h) increase notably for both PPM and secondary inorganic aerosols in most cities and seasons, suggesting that regional transport plays a vital role during haze events. The age information of $PM_{2.5}$, provided by the age-resolved CMAQ model, can help policymakers design effective emergent emission control measures to eliminate severe haze episodes.

1. Introduction

Particulate matter with an aerodynamic diameter ≤ 2.5 μm ($PM_{2.5}$) is the fifth leading mortality risk factor, according to the global burden of disease in 2015 [1]. It can also alter the climate directly by absorbing and scattering solar radiation and indirectly by modifying the microphysical properties of clouds [2]. $PM_{2.5}$ suspended in the atmosphere is a mixture of many components that are either directly emitted (such as elemental carbon (EC) and primary organic aerosols (POA)) or formed through atmospheric chemical processes (such as sulfate, nitrate, ammonium, and secondary organic aerosols (SOA)). During the lifetime of the particles in the atmosphere, their composition, morphology, and optical properties change with atmospheric aging processes, such as chemical transformation, condensation, coagulation, and deposition [3]. At a certain location and time, $PM_{2.5}$ is composed of particles that have been remained in the atmosphere for different amounts of time. The atmospheric age of particles is defined as the total time that has passed since they (or their precursors) were emitted into the atmosphere [4]. Unlike the particles' lifetime, atmospheric age is the instantaneous age of a specific species at a certain location and time. Therefore, it is more relevant to the evolution of the physical and chemical properties of particles rather than the global mean budget. Studying the atmospheric age and age distribution of particles can help us enhance our understanding of the characteristics of $PM_{2.5}$ and assess its associated health and climate impacts.

* Corresponding author.
E-mail address: jianlinhu@nuist.edu.cn (J. Hu).

https://doi.org/10.1016/j.eng.2022.03.013

China has experienced severe haze pollution characterized by extremely high $PM_{2.5}$ loading in recent decades [5,6]. The Chinese government has made great efforts to combat air pollution, including promulgating the Air Pollution Prevention and Control Action Plan in 2013. Recent studies have reported a remarkable decrease in $PM_{2.5}$ concentrations and associated health benefits since 2013 [7]. However, annual $PM_{2.5}$ concentrations in China are still a few times greater than the Guidance Value of the World Health Organization, especially in populous regions such as the North China Plain (NCP), Yangtze River Delta (YRD), and Sichuan Basin (SCB) [8,9]. Therefore, a comprehensive understanding of the formation processes and the source contributions of $PM_{2.5}$ is essential for policymakers to design effective emission control measures. Previous studies have used the receptor model and chemical transport model (CTM) to investigate the source contributions of emission sectors and regions to $PM_{2.5}$ [5,10–14]. However, the time information of particles when they or their precursors are emitted into the atmosphere remains unclear [15].

The atmospheric age of $PM_{2.5}$ can reflect the source–receptor relationship of air pollutants, which provides additional time information on emission sources [4]. For policymakers, knowing such information on air pollutants can help determine the 'optimal' time to conduct emission control measures. A few studies have attempted to estimate the photochemical age of gaseous pollutants based on the reaction rates of non-methane hydrocarbons (NMHCs) or nitrogen oxides (NO_x = NO + NO_2) with hydroxyl (OH) radical [16–18]. This algorithm provides a measure of the extent of a chemical reaction but cannot reflect the actual age of air pollutants (the time since emission). Other researchers used the trajectory model to track the age distribution of particles by adding non-reactive tracers [19,20]. This approach has been further extended to calculate the atmospheric age of NMHCs by implementing a simple chemical scheme that considers the reactions with OH radicals [21]. However, the age distribution calculated by the trajectory model is inaccurate because of the simple treatment of atmospheric chemistry, especially for secondary species. Moreover, the trajectory model does not account for the mixing of air pollutants from different ages and neglects the contribution from background concentrations.

Three-dimensional CTM can simulate the evolution and distribution of chemicals in the atmosphere at global or regional scales, which provides a good basis for estimating the age distribution of air pollutants. Han and Zender [22] estimated the age of dust aerosols using the mass–age tracking (MAT) method in the National Center for Atmospheric Research (NCAR) Community Atmosphere Model version 3 (CAM3). In the MAT algorithm, an additional tracer, the mass–age, was introduced to conserve the aerosol mass and age information. The age of the dust aerosols was then diagnosed by dividing the mass–age by mass. Unfortunately, this method is inadequate for calculating the age distribution of secondary aerosol species owing to the complex nonlinear chemical process. Wagstrom and Pandis [4] used the regional CTM PMCAMx to track the age distribution of aerosols. Particles and their precursors emitted at different times were assigned to separate bins, that is, emission time periods (ETPs), and treated as different source categories by the Particulate Matter Source Apportionment Technology (PSAT). However, this method is not suitable for long-term simulations because the computational time increases sharply with the number of ETPs. To overcome this limitation, Ying et al. [23] introduced a dynamic time-bin advancing technique to track the age distribution of primary $PM_{2.5}$ (PPM) and secondary inorganic aerosols (sulfate, nitrate, and ammonium, simply SNA hereafter) in a source-oriented the community multiscale air quality (CMAQ) model framework. Based on this technique, we further developed a source- and age-resolved algorithm (SARA) into the CMAQ model to track the age distribution of $PM_{2.5}$, as well as its source sector and source region contributions during the 2013 January severe haze episode in China [24].

Although the above studies have investigated the age distribution of particles in different locations, these studies mostly focused on single pollution episodes, and few have attempted to address the seasonal variations in the age distribution of $PM_{2.5}$. In this study, the age-resolved CMAQ model was applied to track the spatial and seasonal variations in the age distribution of the predominant $PM_{2.5}$ components, PPM and SNA, in China in the entire year 2013. Secondary organic aerosols (SOA) are not considered because their concentrations are generally underestimated by current air quality models [25]. The results of this study will provide valuable information on the age distribution of $PM_{2.5}$ in different regions and seasons, which can help policymakers design timely control measures to effectively reduce $PM_{2.5}$.

2. Methods

2.1. Model description and setups

The CMAQ model was originally developed by the US Environmental Protection Agency (EPA) [26] and has been used around the world to simulate air pollutants, including tropospheric ozone (O_3) and $PM_{2.5}$, at regional and urban scales [27–29]. The CMAQ model has also been applied in China to investigate the formation mechanisms, source contributions, control strategies, and health impacts of $PM_{2.5}$ pollutions in various regions [30–33]. In this study, the CMAQ model version 5.0.1 coupled with the SAPRC-07 photochemical mechanism and the 6th version of the aerosol module (AERO6) was applied to simulate atmospheric chemistry. The model configurations were mainly derived from Hu et al. [30], in which several modifications were implemented in the CMAQ model to improve the model performance for predicting secondary inorganic and organic aerosols. The heterogeneous pathways of secondary sulfate and nitrate formation on the particle surface from nitrogen dioxide (NO_2) and sulfur dioxide (SO_2) were added to the original CMAQ model [34], which helped correct the underestimation of sulfate and nitrate especially under severe haze conditions [35]. In addition, detailed treatments of SOA formation were adopted, including isoprene oxidation chemistry, in-cloud processing of glyoxal and methylglyoxal, and aerosol surface uptake of isoprene epoxydiol and methacrylic acid epoxide [36–38]. More information about the above updates and their benefits can be found in the cited references.

The simulation domain covers all of China and its adjacent countries in eastern Asia, with a horizontal grid resolution of 36 km (Fig. 1). The Weather Research Forecasting (WRF) model version 4.2 was used to generate the offline meteorological input, with the initial and boundary conditions from the 1.0° × 1.0° National Centers for Environmental Prediction (NCEP) Final (FNL) operational global reanalysis data. Details of the WRF configurations have been documented in previous studies [30,39] and are not repeated here. The emission inputs for the CMAQ model in this study include anthropogenic and natural inventory data. The anthropogenic emissions in China were derived from the monthly based Multi-resolution Emission Inventory for China (MEIC) version 1.3[†] with 0.25° × 0.25° resolution [40], while emissions outside China within the model domain were obtained from the monthly gridded Regional Emission inventory in ASia version 3.2 (REASv3.2) with 0.25° × 0.25° resolution [41]. The weekly and diurnal profiles used to generate hourly emissions were described in detail by Zhang et al. [39]. Biogenic emissions were calculated using the Model of Emissions of Gaseous and Aerosols from Nature

[†] https://www.meicmodel.org

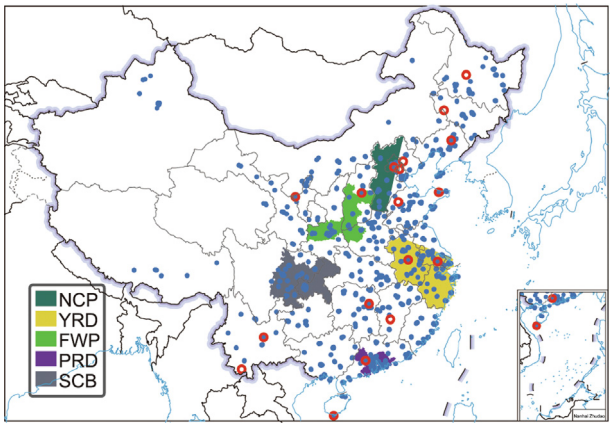

Fig. 1. Model domain. The blue circles indicate the locations of cities with air quality observations. The red circles show the locations of sites from the Campaign on Atmospheric Aerosol Research network of China (CARE-China). Five sub-regions discussed in the text are also shown in the figure. NCP represents the North China Plain, YRD represents the Yangtze River Delta, FWP represents the Fenwei Plain, PRD represents the Pearl River Delta, and SCB represents the Sichuan Basin.

(MEGAN) v2.10 [42] driven by meteorological fields predicted by the WRF model. The Fire INventory from NCAR (FINN) version 1.5 with 1 km resolution [43] was applied for open biomass burning emissions. The natural emissions of dust and sea salt were calculated in line by the CMAQ model. As shown in Fig. S1 in Appendix A, emissions are much higher in NCP, Fenwei Plain (FWP), YRD, and SCB. Seasonally, SO_2, NO_x, and PPM emissions are higher during winter in NCP, FWP, and SCB, but NH_3 emissions are higher during summer over most parts of China.

2.2. Description of age-resolved algorithm

The CMAQ model was modified to track the atmospheric age distribution of primary and secondary $PM_{2.5}$, using additional tagged species and reactions. The age-resolved algorithm was developed based on the source-oriented externally mixed aerosol representation framework and was initially applied in the University of California at Davis (UCD)/California Institute of Technology (CIT) air quality model to track the age distribution of EC in Texas, USA [44]. Ying et al. [23] further expanded the age-resolved algorithm to track the atmospheric age distribution of SNA and introduced the algorithm into the CMAQ model version 5.0.1. This algorithm, as described below, was applied in this study.

Species with different atmospheric ages were assigned to different time bins by adding tagged species to the age-resolved CMAQ model. Species in different age bins were assumed to have the same physical and chemical properties. For PPM, tagged non-reactive tracer ATCR_X_0 was added to represent the freshly emitted PPM particles with atmospheric age less than the predefined fixed age bin advancing frequency ($\Delta\tau$ = 12 h in this study). PPM concentrations from emissions at the current model time step were always set to the first age bin (ATCR_X_0) and were sequentially moved to the next age bin (i.e., ATCR_X_1, ATCR_X_2, …, ATCR_X_n) every 12 h (equal to the age bin advancing frequency); where n represents the number of age bin. In this study, n was set to 9, and a total of ten age bins were tracked. The last age bin ATCR_X_9 represents PPM with an atmospheric age $\geq$ 108 h. The emission rates of PPM were the total of individual PPM components (such as EC and primary organic carbon) and scaled by 0.001% [10].

The age distribution of SNA is more complicated to determine in the age-resolved CMAQ model, which is calculated based on the emissions of the corresponding gaseous precursors such as SO_2, nitrogen oxides (NO_x), and ammonia (NH_3). Additional tagged species and reactions were introduced into the original SAPRC-07 mechanism, while the aerosol and cloud modules were also updated to include the treatments for tagged SNA species. For example, sulfate formation through the gas-phase reaction of SO_2 oxidation by OH radicals can be expanded into several similar reactions:

$$SO_2\_X_0 + OH \rightarrow H_2SO_4\_X_0 \rightarrow S(VI)\_X_0 \text{ (Reaction 1)}$$

$$SO_2\_X_1 + OH \rightarrow H_2SO_4\_X_1 \rightarrow S(VI)\_X_1 \text{ (Reaction 2)}$$

$$\vdots$$

$$SO_2\_X_n + OH \rightarrow H_2SO_4\_X_n \rightarrow S(VI)\_X_n \text{ (Reaction 3)}$$

where $SO_2\_X_i$, $H_2SO_4\_X_i$, and $S(VI)\_X_i$ represent the SO_2, gas-phase sulfate, and particulate sulfate in the ith age bin, respectively. Similar to PPM, the concentrations in each age bin were updated using a dynamic age bin advancing technique. Specifically, the concentrations in the ith age bin were moved to $(i + 1)$th age bin every 12 h.

Once the atmospheric age distribution of a specific species was tracked in the age-resolved CMAQ model, the average atmospheric age ($\bar{\tau}$) of PPM and SNA can be calculated by the average of the concentration-weighted age in each age bin, expressed by Eq. (1). The details can be found in Ying et al. [23].

$$\bar{\tau} = \sum_{i=0}^{n} \frac{\bar{\tau}_i \times C_i}{\sum_{i=0}^{n} C_i} \tag{1}$$

where C_i is the concentration of specific species in the ith age bin. $\bar{\tau}_i$ represents the average atmospheric age in the ith age bin, which is equal to the middle of the corresponding time period:

$$\bar{\tau}_i = \left(i + \frac{1}{2}\right)\Delta\tau \qquad i = 0, 1, 2, \cdots, n \tag{2}$$

2.3. Model evaluation data and metrics

Two observational datasets were used for the model evaluation in this study. The first is the hourly $PM_{2.5}$, obtained from the publishing website of the China Ministry of Ecology and Environment (MEE)[†]. This network includes 496 monitoring stations in 74 major cities since January 2013, as shown in Fig. 1. The second is the monthly sulfate, nitrate, and ammonium concentrations at 18 stations across China during 2013 (see Fig. 1). These data were derived from the extended data of Zhai et al. [45][‡], which was originally measured by ion chromatography from the Campaign on Atmospheric Aerosol Research network of China (CARE-China) [46,47]. Details of the network stations, instrumentation, and methodologies are described in the cited references.

The statistical metrics calculated for model evaluation include the mean fractional bias (MFB), mean fractional error (MFE), normalized mean bias (NMB), normalized mean error (NME), root mean square error (RMSE), and correlation coefficient (R). More information about the calculation of the metrics and the model performance criteria can be found in Emery et al. [48] and is not repeated here.

3. Results

3.1. Model evaluation

Meteorological parameters such as temperature, relative humidity, wind speed, and wind direction predicted by the WRF

[†] https://106.37.208.233:20035/.
[‡] https://doi.org/10.7910/DVN/VHFTLQ.

model for the entire year of 2013 were evaluated against observations in China [30], and the accuracy of the model performance was determined to be acceptable according to benchmarks suggested by Emery et al. [49]. Hu et al. [30] also evaluated the model performance on O_3 and $PM_{2.5}$, simulated by the original CMAQ model, and found that the NMB, NME, MFB, and MFE for O_3 and $PM_{2.5}$ met the performance criteria in most cities for most months. In this section, we compare the seasonal and monthly averaged $PM_{2.5}$, sulfate, nitrate, and ammonium concentrations predicted by the age-resolved CMAQ model with measurements.

Fig. 2 shows the regional distributions of the simulated and observed $PM_{2.5}$, sulfate, nitrate, and ammonium concentrations during the four seasons of 2013. The corresponding model performance statistics are presented in Table 1 [48]. The overall model performance for $PM_{2.5}$ and SNA meets the criteria for satisfactory performance ($-30\% \leq$ NMB $\leq 30\%$, NME $\leq 50\%$, and $R > 0.4$ for $PM_{2.5}$, sulfate, and ammonium; $-65\% \leq$ NMB $\leq 65\%$ and NME $\leq 115\%$ for nitrate) suggested by Emery et al. [48]. Negative NMB of $PM_{2.5}$ is found in spring, summer, and autumn, indicating that the model underestimated $PM_{2.5}$. Sulfate, nitrate, and ammonium concentrations are overestimated in all seasons, with mean NMB values of 24.0%, 43.9%, and 15.2%, respectively. For sulfate, relatively poor model performance is found in autumn, with both NMB and NME exceeding the performance criteria. The NMB and NME of nitrate (34.3%–55.6% for NMB and 60.3%–83.0% for NME) are relatively larger than those of sulfate, although they are all within the performance criteria. The NMB of ammonium (8.3%–21.7%) is considerably better than that of sulfate and the NME (36.4%–55.0%) is similar to that of sulfate.

The predicted and observed $PM_{2.5}$, sulfate, nitrate, and ammonium exhibit consistent seasonal variations, with high concentrations in winter and low concentrations in summer. For example, the simulated summer SNA is 18.6 $\mu g \cdot m^{-3}$, contributing to a larger fraction (46.5%) of $PM_{2.5}$ than during the winter season (36.2%). Such seasonal variation is consistent with the observations and previous study [50] and is mainly attributed to the enhanced photochemical formation of secondary aerosols under the influence of high O_3 levels and strong solar radiation in summer [51]. The model correctly predicts high $PM_{2.5}$ and SNA concentrations in the NCP and eastern region of China, especially in winter and autumn. $PM_{2.5}$ concentrations in those areas are even higher than 200 $\mu g \cdot m^{-3}$ in winter, considerably higher than the Chinese Ambient Air Quality Standards (CAAQS) Grade II standard for daily average $PM_{2.5}$ (75 $\mu g \cdot m^{-3}$). However, in winter and autumn, the model tends to underestimate the $PM_{2.5}$ concentrations in the FWP and overestimate in the SCB, consistent with previous studies [31]. The biases are partially due to the coarse horizontal resolution (36 km) used in this study, which cannot accurately predict wind speed, precipitation, and other meteorological parameters in such a complex topography [52]. Other reasons might be the uncertainties in emissions and the numerical representation of heterogeneous reactions [30].

Fig. 3 compares the predicted monthly averaged $PM_{2.5}$, sulfate, nitrate, and ammonium concentrations with observations at individual sites. Overall, the model agrees well with the observations in most regions for most months, with high correlation coefficients ($R \geq 0.75$, $p < 0.001$) and relatively low biases (< 5% for $PM_{2.5}$, and < 45% for SNA). However, the $PM_{2.5}$ concentrations are underestimated by 4.3%, while the simulated SNA concentrations are overestimated by 16.6%–42.8%, especially for nitrate. Such different biases are partially due to the uncertainties associated with the model treatments. For example, current air quality models significantly underestimate SOA in China because of limitations in understanding the complicated SOA formation mechanism, such as the contribution of intermediate-volatility or semi-volatile organic compounds [25,53]. Other possible reasons for model-to-observation discrepancy lie in the uncertainties in the emission inventory, the relatively coarse model grid resolution, and the unavoidable deficiencies in simulated meteorological fields such as wind speed [7,30]. The predicted sulfur oxidation ratio (SOR), nitrogen oxidation ratio (NOR), and SNA to EC ratio (SNA/EC), which are frequently used as indicators for assessing the extent of SNA formation, are further compared with observations (Fig. S2 in Appendix A). Generally, the correlation coefficients for SOR and NOR are found to be 0.55 and 0.52, respectively, indicating that the model successfully reproduces the chemical formation process of sulfate and nitrate. Nonetheless, the model overestimates SOR and NOR by 37.5% and 26.4%, respectively. The model performance for SNA/EC is satisfactory with a relatively high correlation coefficient and low bias (R = 0.54, NMB = −7.2%).

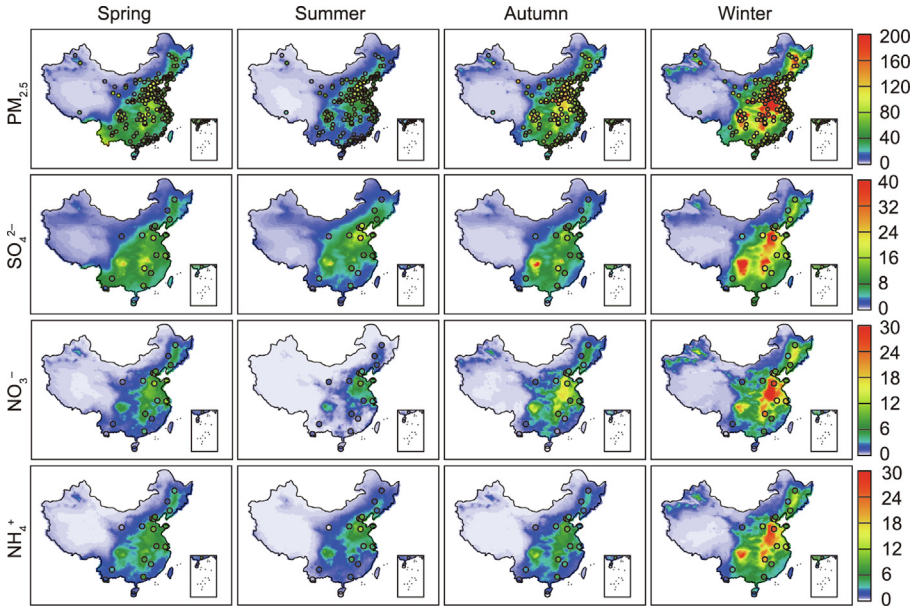

Fig. 2. Comparison of predicted (contour) and observed (dotted) $PM_{2.5}$, sulfate (SO_4^{2-}), nitrate (NO_3^-), and ammonium (NH_4^+) in Spring, Summer, Autumn, and Winter of 2013. Unit: $\mu g \cdot m^{-3}$.

Table 1
Model performance statistics of $PM_{2.5}$, sulfate (SO_4^{2-}), nitrate (NO_3^-), and ammonium (NH_4^+) in different seasons of 2013.

Item	Season	OBS ($\mu g \cdot m^{-3}$)	SIM ($\mu g \cdot m^{-3}$)	MFB (%)	MFE (%)	NMB (%)	NME (%)	RMSE ($\mu g \cdot m^{-3}$)	*R*
$PM_{2.5}$	Spring	64.3	53.6	−24.8	37.2	−16.6	31.6	26.3	0.6
	Summer	46.4	40.1	−23.7	41.0	−13.5	33.1	20.5	0.7
	Autumn	73.2	69.8	−14.7	40.3	−4.6	37.4	38.6	0.5
	Winter	113.8	117.6	−8.2	34.5	3.3	32.2	50.2	0.7
SO_4^{2-}	Spring	8.2	9.1	12.6	41.6	11.4	43.1	4.8	0.6
	Summer	8.6	10.2	25.3	46.6	19.1	42.3	5.6	0.7
	Autumn	7.8	10.5	36.8	58.5	**34.9**	**61.8**	6.4	0.5
	Winter	13.9	18.2	23.7	45.3	**30.7**	48.0	9.3	0.8
NO_3^-	Spring	5.0	6.7	24.7	63.4	34.3	60.9	4.4	0.6
	Summer	2.8	4.0	0.6	84.7	43.3	83.0	3.4	0.7
	Autumn	3.8	5.9	35.5	77.8	55.6	81.3	4.5	0.7
	Winter	9.5	13.5	37.2	58.4	42.2	60.3	8.0	0.8
NH_4^+	Spring	4.7	5.3	14.6	45.2	12.7	43.0	2.8	0.6
	Summer	4.1	4.4	22.7	56.1	8.3	46.6	2.7	0.7
	Autumn	3.7	4.4	26.4	57.6	18.0	**55.0**	2.9	0.6
	Winter	8.9	10.8	26.3	39.7	21.7	36.4	4.6	0.9

OBS: mean observation; SIM: mean simulation. The values that do not meet the performance criteria ($-30\% \le NMB \le 30\%$, $NME \le 50\%$, and $R > 0.4$ for $PM_{2.5}$, sulfate, and ammonium; $-65\% \le NMB \le 65\%$ and $NME \le 115\%$ for nitrate) suggested by Emery et al. [48] are denoted in bold.

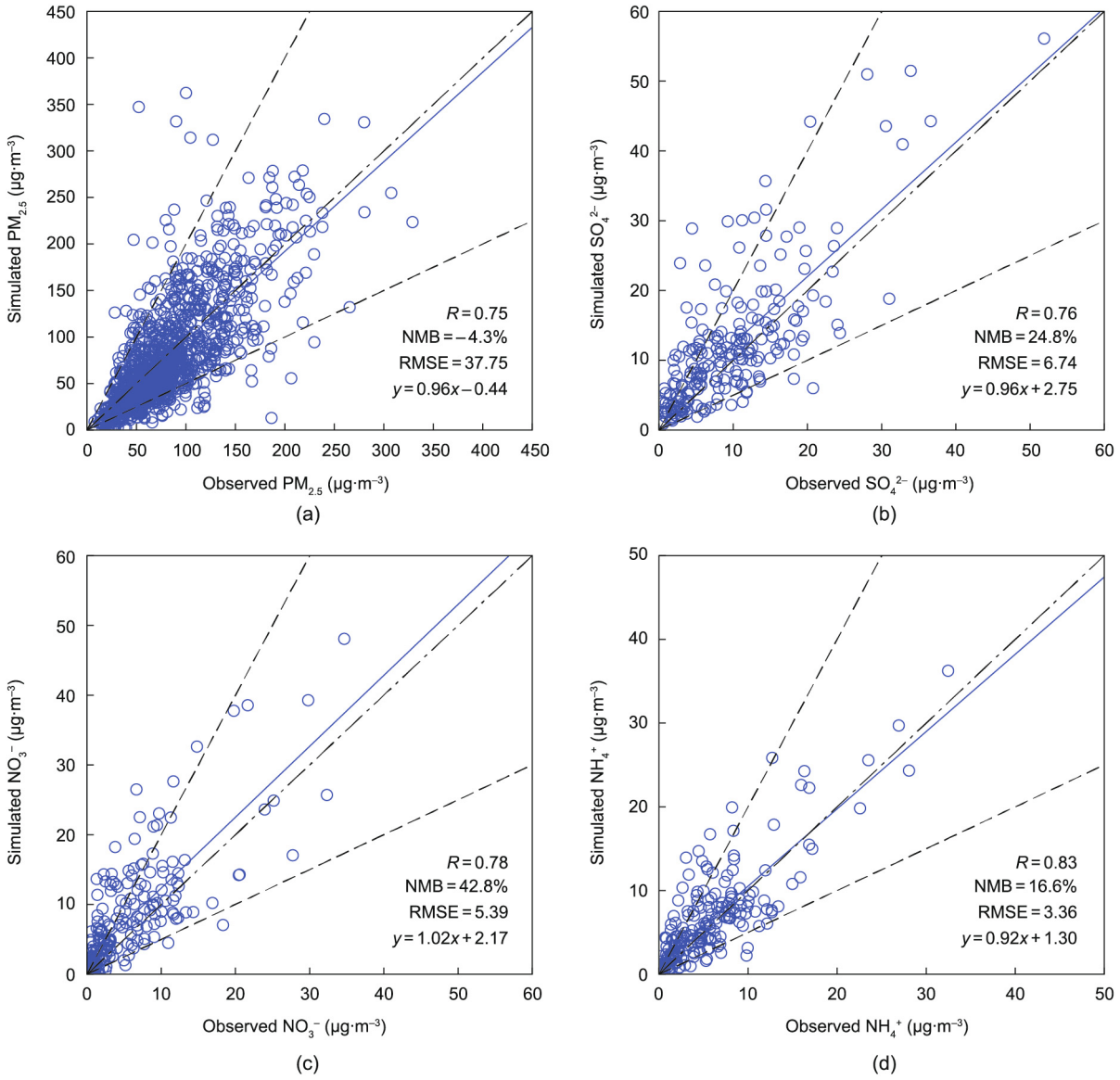

Fig. 3. Comparison of predicted and observed monthly averaged (a) $PM_{2.5}$, (b) sulfate, (c) nitrate, and (d) ammonium in 2013.

3.2. Seasonal variations and regional distributions of atmospheric age

The spatial distributions of seasonally averaged PPM concentrations in different age bins, together with the averaged wind fields, are illustrated in Fig. 4. Overall, PPM mainly originates from fresh local emissions, with the overwhelming majority concentrated in the 0–12 and 12–24 h age groups in all four seasons. Freshly emitted PPM is spatially limited in the source regions within 24 h and gradually transported to downwind areas with increasing age. Using the Nested Air Quality Prediction Model System (NAQPMS), Chen et al. [54] also found a low aging time scale (several hours) of black carbon in Beijing but with much higher values (> 1.2 days) in remote regions far from the source areas. In addition, the atmospheric age distributions in different regions show remarkable seasonal variations. In spring, high concentrations of fresh PPM with atmospheric age ≤ 12 h are observed in Southeast Asia, with a maximum exceeding 35 μg·m^{-3}. This is mainly attributed to intensive primary emissions (Fig. S1) related to open biomass burning of agricultural waste and forest fires in these areas [55]. Relatively high concentrations (~20 μg·m^{-3}) of fresh PPM with age ≤ 12 h are also predicted in densely urbanized areas such as the NCP, SCB, and YRD due to intensive local emissions and low wind speed. As the atmospheric age increased, the PPM concentrations in the emission regions decrease significantly due to horizontal and vertical dispersion as well as deposition processes. The peak value in South Asia decreases to only 5 μg·m^{-3} for PPM in the > 96 h age group. In contrast, PPM concentrations in Guangxi, Guangdong, and Yunnan Regions, and the South China Sea remain high for the 48–96 h and > 96 h age groups, indicating the impact of long-range transport.

In summer, high fresh PPM (≤ 12 h) concentrations of about 15 μg·m^{-3} are located in the NCP, YRD, and SCB. PPM concentrations in southern China decrease rapidly after 24 h of aging, while the concentrations within the 48–96 h age group are still relatively high in the NCP. Due to prevailing winds from the south, freshly emitted PPM extends from central and southern China to the NCP and accumulated in the NCP areas because of the blocking effect of the Taihang and Yanshan Mountains in the north and west [56]. In autumn, the spatial distribution of freshly emitted PPM is similar to that in summer but with relatively higher concentrations due to increased anthropogenic emissions [57]. Under prevailing northerly winds, PPM particles tend to spread southerly with increasing atmospheric age. The PPM concentrations in the 48–96 h age bin remain about 5 μg·m^{-3} in Yunnan Province, which is considerably higher than the summer concentrations. In winter, high concentrations (~35 μg·m^{-3}) of PPM with age < 24 h are observed in the NCP, SCB, and northeast China (NE). This is mainly attributed to the enhanced residential emissions from coal combustion for domestic heating and the unfavorable meteorological conditions associated with low wind speed and mixing height [58].

Fig. 5 shows the regional distributions of the seasonal average SNA concentrations in different age bins. Generally, the age distribution of the SNA exhibits significant seasonal variations. In spring, the concentrations of SNA in the first two age bins are almost the same, with a peak value of 25 μg·m^{-3} in the SCB and Hunan Province. The concentrations of SNA decrease rapidly after 24 h and spread over a wide area. The concentrations of aged SNA with atmospheric age > 96 h remain relatively high (2–5 μg·m^{-3}) in southern and central China, which is explained by its relation to sulfate (Fig. S3 in Appendix A). In summer, high SNA concentrations are observed in

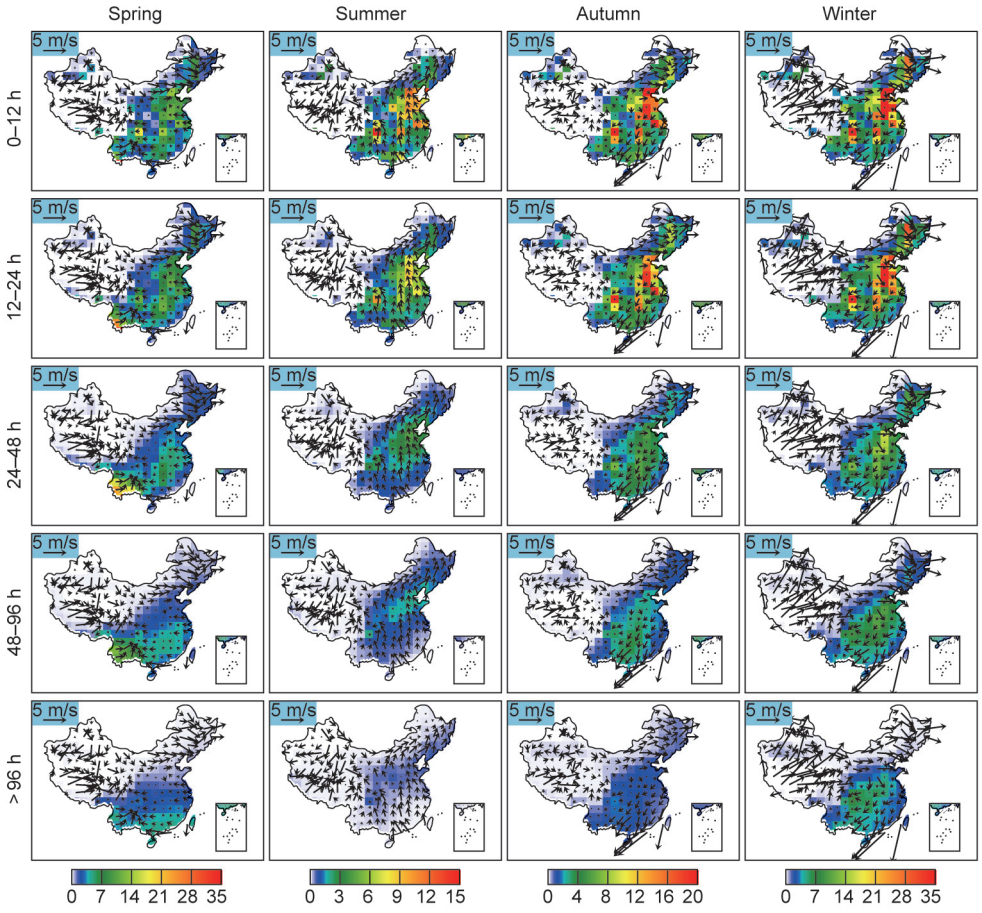

Fig. 4. Seasonal mean PPM concentrations (μg·m^{-3}) in different age bins overlapped with wind vectors.

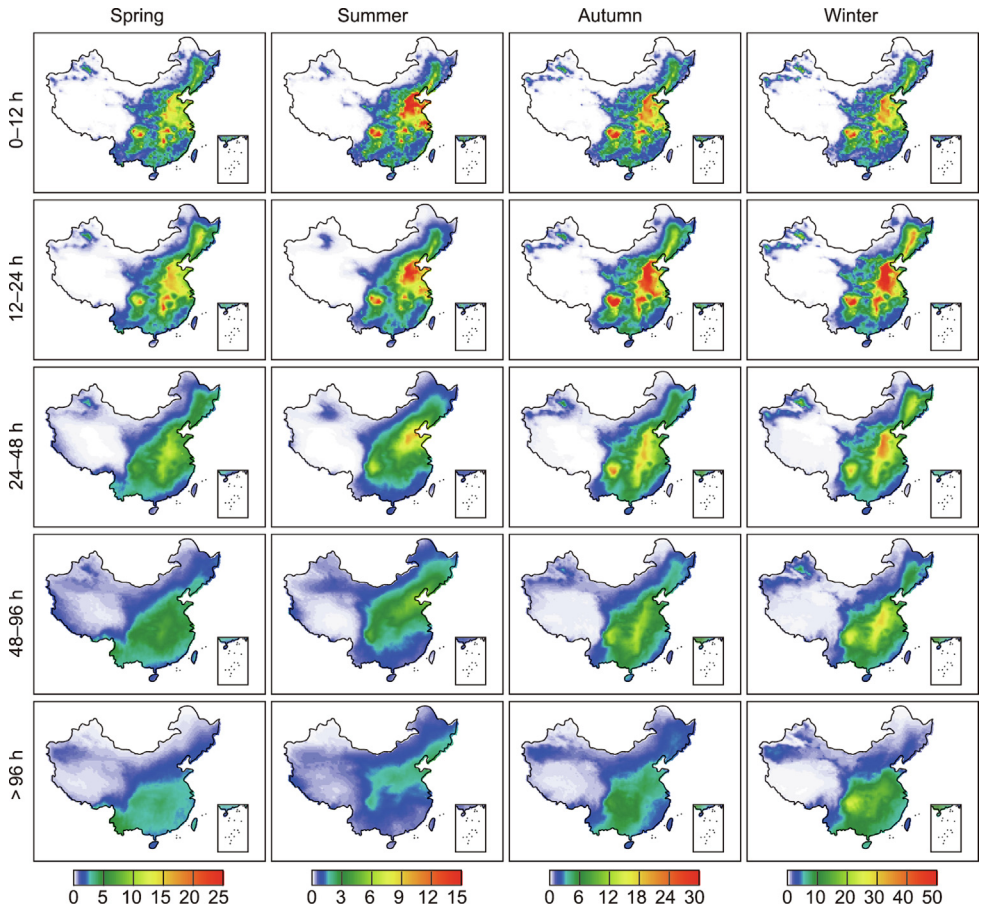

Fig. 5. Seasonal variation of secondary inorganic aerosol (SNA) concentrations ($\mu g \cdot m^{-3}$) in different age bins.

the first age bin, with a maximum concentration of 15 $\mu g \cdot m^{-3}$ in the NCP, SCB, and YRD. This reduction in atmospheric age is because of high summer temperature and solar radiation, which promotes the atmospheric oxidation capacity and facilitates the gas-to-particle conversion rate [59]. This is consistent with a previous study, which shows the photochemical age in summer is only 1.2–3.5 h [60]. Similar to PPM, SNA concentrations gradually decrease as the atmospheric age increased. The aged SNA tends to be concentrated in northern China and the Yellow Sea under prevailing southerly winds. As such, in autumn and winter, high concentrations of SNA can be found in the 12–24 h age bin, with a maximum of 30 and 50 $\mu g \cdot m^{-3}$, respectively. This is because the gas-phase reactions of SO_2 and NO_x are considerably slower in these seasons (Figs. S4 and S5 in Appendix A), leading to an older atmospheric age. Additionally, fresh SNA particles are concentrated in source regions such as the NCP, SCB, and central China owing to low wind speed and shallow mixing layers. For older age groups, SNA can be transported southerly under the prevailing northerly wind, and its concentrations remain high in central China and the SCB.

The spatial distributions of seasonally averaged sulfate, nitrate, and ammonium concentrations for different age groups are shown in Figs. S3–S5. The fresh sulfate and nitrate concentrations with an atmospheric age of 0–12 h are relatively low and spatially limited in the source regions. Sulfate and nitrate in older age groups show a smooth spatial distribution with weaker concentration gradients. High concentrations of sulfate can be observed in the 12–24 h and even 24–48 h age groups because of the long lifetime of SO_2 (Fig. S6 in Appendix A) [61]. In winter, the concentrations of sulfate with atmospheric age > 96 h are still high in the SCB, with a maximum of 15 $\mu g \cdot m^{-3}$. The predicted nitrate concentrations are highest in the 12–24 h age group for all four seasons and rapidly decrease after 24 h. This is because the lifetime of NO_x is considerably shorter than that of SO_2 (Figs. S6 and S7 in Appendix A) [23,62]. The aged nitrate is likely due to the longer lifetime of NO_z (Fig. S8 in Appendix A), such as peroxyacetyl nitrate (PAN), which can be transported to remote regions and release NO_x [63]. Most ammonium is concentrated in the 0–12 h age group and limited in the source region. This is mainly attributed to the shorter lifetime of NH_3 as shown in Fig. S9 in Appendix A, which indicates NH_3 can be quickly transformed to ammonium. The gas-particle partitioning of NH_3 to ammonium is limited by the availability of either NH_3 or HNO_3, which can be represented by the adjusted gas ratio (adjGR) [64]. As can be seen from Fig. S10 in Appendix A, wintertime adjGR is lower than one in most parts of eastern China, indicating that NH_3 is in short and can rapidly convert to ammonium in a short time. Based on Peking University NH_3 (PKU-NH_3) emission inventory and WRF-Chem simulation, Liu et al. [65] also found NH_3-limited conditions during winter haze days due to the rapidly increased nitrate concentrations. However, adjGR is found to be higher than one during summer, with high values in southwestern China and low values in the NCP. The high adjGR values in summer indicate NH_3 is abundant, which is mainly due to agricultural activities. Previous studies also showed enhanced NH_3 emissions in summer, leading to NH_3-rich regimes [66].

Fig. 6 shows the spatial distribution of the average atmospheric age of PPM, sulfate, nitrate, and ammonium in different seasons. For PPM, a low atmospheric age is observed in the NCP, YRD, SCB, and NE for all four seasons, which is mainly related to intensive local emissions. The average age of PPM in the NCP and NE is about 20 h during winter, which is slightly lower than that during summer (~25 h). In contrast, in southern and central China, PPM shows a much older age in winter than in summer, with a maximum

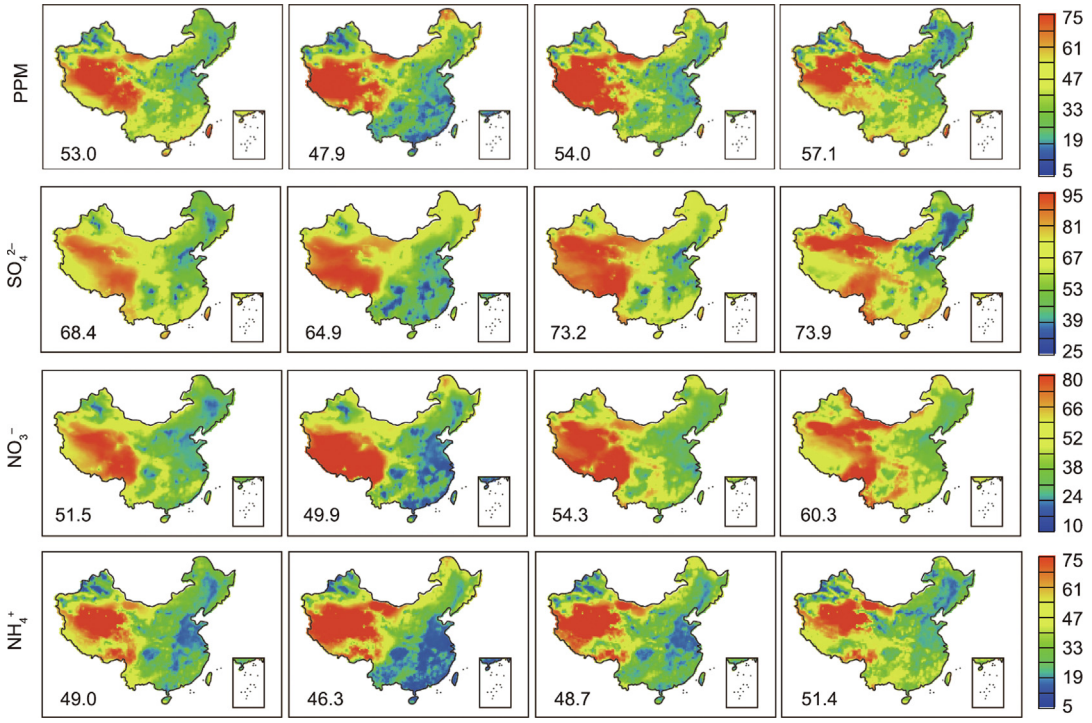

Fig. 6. Seasonal variation of predicted average atmospheric age (in hours) of PPM, sulfate, nitrate, and ammonium. The number in each panel indicates the domain averaged value.

difference greater than 48 h in Yunnan and Guangxi Provinces. As shown in Fig. 4, this is mainly attributed to the transition in the wind direction during different monsoon seasons. Old PPM particles are transported southerly in winter under prevailing northerly winds, while they accumulate in the NCP and NE in summer.

The average age of sulfate is significantly higher than that of the PPM. In spring, a low sulfate age is observed in the NCP, NE, SCB, and central China, with a minimum of ~25 h. The average age is considerably higher in western China and remote oceans because of the low emissions in these regions. In summer, the average age of sulfate is remarkably lower in southeastern coastal areas, such as Guangzhou, Fujian, and Zhejiang Provinces. The low ages in these regions are partly attributed to the strong southerly winds in summer (Fig. 4), which quickly disperse air pollutants in these regions. Another possible reason is the enhanced gas-to-particle conversion rate of SO_2 because of the higher temperature and radiation in summer and the increased deposition removal due to increased summer precipitation (Fig. S11 in Appendix A). In winter, the average atmospheric age of sulfate exhibits a significant north-to-south gradient. The average age is close to 25 h in the NCP and NE, while it reaches up to 80 h in southern China. As such, the low average age in the NCP and NE is attributed to the fresh emissions of primary sulfate from residential heating and cooking with coal. Moreover, the gas-phase oxidation of SO_2 initiated by OH radicals is very slow in winter; thus, SO_2 can be transported over a longer distance and time and lead to a high age in southern China. The atmospheric age of nitrate is lowest in summer and highest in winter, partly because of the shorter atmospheric lifetime of NO_x in summer than in winter [62]. Another reason is the higher temperature in summer, which leads to more nitrate partitioning into the gas phase. Because nitric acid in the gas phase deposits faster than particulate nitrate [67], a lower atmospheric age can be found in summer. Significant seasonal variations in nitrate age are observed in southern China. In the PRD, nitrate has an average age of about 15 h during summer, while its average age increases to 45–50 h during winter. Moreover, ammonium shows a lower atmospheric age than sulfate and nitrate due to the short NH_3 lifetime of the order of hours [68]. The spatial distribution and seasonal variation of the atmospheric age of ammonium are similar to those of the PPM. The average age of ammonium is even lower than that of PPM in eastern China because of the larger removal rate of dry and wet deposition (Fig. S11).

Fig. 7 shows the simulated seasonal age distribution and mean atmospheric age averaged over five key regions (shown in Fig. 1), including the NCP, FWP, YRD, PRD, and SCB. For PPM, sulfate, and ammonium, the age distributions in the NCP and FWP are moderately different from those in other regions, with a relatively small seasonal difference (< 6.5 h). The average age of PPM and ammonium is approximately 20–30 h in the NCP and FWP, while the sulfate average age is significantly larger (40–56 h). In the NCP, the highest average age is found in autumn, while the lowest was found in winter. In contrast, significant seasonal variations in atmospheric age are observed in the YRD, PRD, and SCB, with a higher average age in winter and a lower average age in summer. For example, in the PRD, the average age of PPM and ammonium can increase from about 15 h in summer to about 40 h in winter. This regional difference in seasonal variation in atmospheric age is mainly attributed to the changing wind speed and direction. In summer, the prevailing southerly wind brings aged pollutants to the NCP, while in the winter, pollutants are transported to downwind areas under the northerly wind. For nitrate, the contributions from old age groups (> 24 h) in winter range from 40% to 60%, which is significantly higher than that in summer. The average age in winter is considerably larger than that in summer for all five regions, especially in the PRD. The average age of nitrate is 18–30 h in summer, while it increases to 35–50 h for all regions. The higher temperature in summer favors nitrate partitioning to the gas phase, which leads to faster deposition and reduces atmospheric age [45,67].

3.3. Atmospheric age distribution on pollution days

Fig. 8 illustrates the age distribution of PPM and SNA on pollution days ($\geq$ 75 $\mu g \cdot m^{-3}$) and clean days (< 75 $\mu g \cdot m^{-3}$) in five

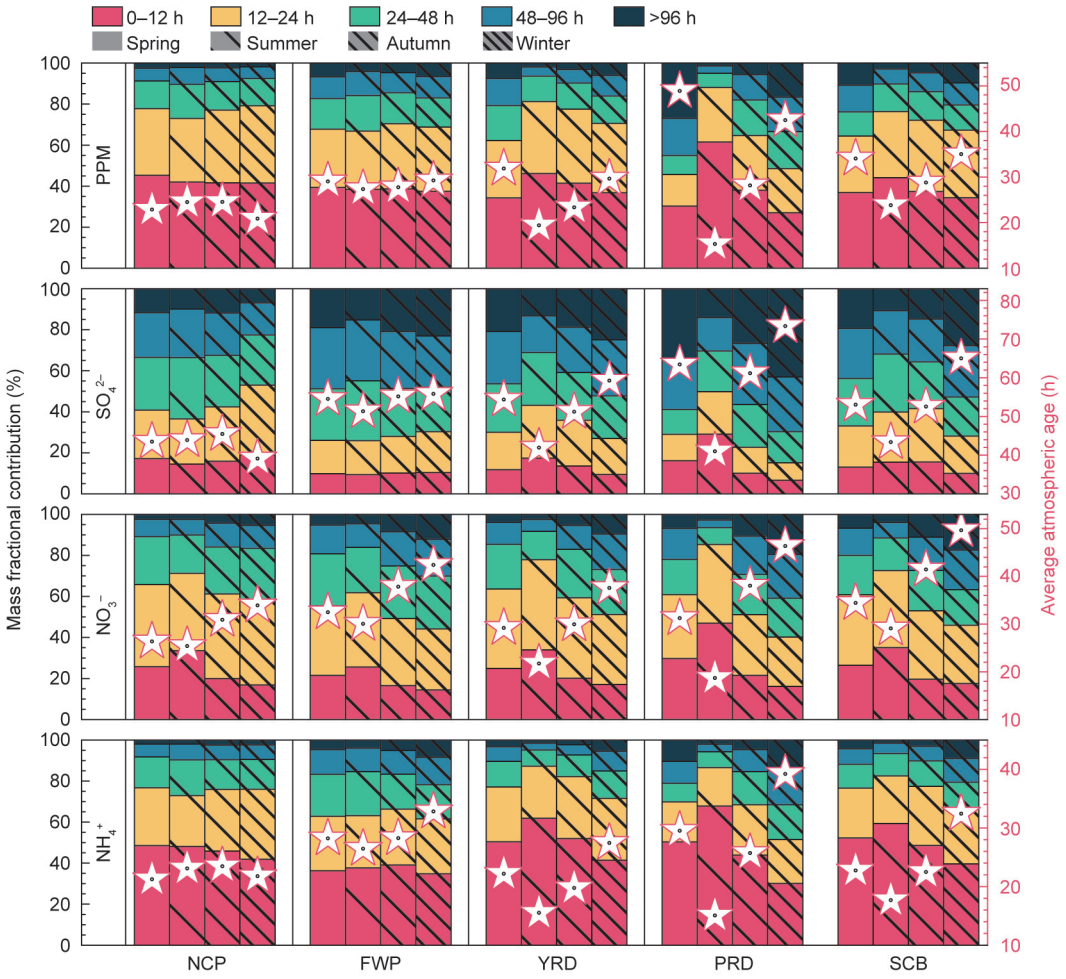

Fig. 7. The mass fractional contributions of different age bins to PPM, sulfate, nitrate, and ammonium over five key regions. The red star with a black dot indicates the average atmospheric age (in hours, right *y*-axis).

megacities: Beijing, Shanghai, Guangzhou, Chongqing, and Xi'an (representing NCP, YRD, PRD, SCB, and FWP, respectively). In most cities and seasons, the average age of PPM and SNA increases significantly on pollution days, with a maximum increment of approximately 24 h. Taking Beijing as an example, the average age of PPM in winter increases from 10 h on clean days to 28 h on pollution days. The accumulation of local emissions due to unfavorable meteorological conditions and the enhanced contribution from regional transport can both lead to increased aerosol age during pollution days [5,58]. Fig. S12 in Appendix A further illustrates the day-to-day variations in the age distribution of PPM, sulfate, nitrate, and ammonium in Beijing in January (winter) and July (summer). The contributions of 0–24 h age bins are more than 90% to the total PPM concentrations on clean days (e.g. January 1–8, and July 2–4), while the contributions from older age bins (> 24 h) increase significantly during high concentration days (e.g., January 28–30, and July 6–8). This is linked to the persistent stagnation conditions associated with low wind speed and shallow mixing height, which trap both fresh particles from local emissions and aged particles transported from other regions for a long time. Sulfate particles with an atmospheric age of 24–96 h account for only 10%–20% of the total sulfate on clean days, such as July 2–5, while their contribution increases to 60%–75% during high concentration days (e.g., July 18–21). On the peak concentration day, January 31, sulfate particles in the 48–96 and 24–48 h age bins account for 37% and 25% of the total sulfate respectively. For nitrate, the contributions of > 24 h age bins usually increase significantly during relatively high nitrate concentration days, such as January 4–7 and July 26–27. In contrast, nitrate concentrations increase rapidly during January 16–20, while the contributions of aged nitrate particles (> 48 h) remain almost unchanged. Similar to PPM, the contribution of aged ammonium particles (> 48 h) greatly increases with the total mass concentration, with a maximum of 41.6% on the peak concentration day, January 31.

Some cities, such as Shanghai, show less difference in the age distribution of SNA between pollution days and clean days in spring and summer. However, in winter, pollution days have more aged particles (> 24 h) and a larger average age of both PPM and SNA. For example, the average age of SNA increases from 30 h on clean days to 48 h on pollution days in winter. As shown in Fig. S13 in Appendix A, northwesterly winds from central China and NCP usually lead to increased particle concentrations in January, which is associated with a high contribution of old age bins. PPM particles from the 48–96 h and > 96 h age bins account for approximately 20% of the total concentrations in January, especially during high concentration days. For example, as the PPM concentration increases from about 8 $\mu g \cdot m^{-3}$ on January 3 to 47 $\mu g \cdot m^{-3}$ on January 7, the contribution of old age bins (> 48 h) gradually increases from less than 1% to approximately 20%. A similar phenomenon can also be observed for sulfate, nitrate, and ammonium. In July, most PPM particles originate from the 0–12 h age bin due to southeasterly wind, which brings in clean air from the ocean and is beneficial to the removal of freshly emitted PPM particles. The sulfate concentration in January reaches 20 $\mu g \cdot m^{-3}$ on a few days, with a peak value of

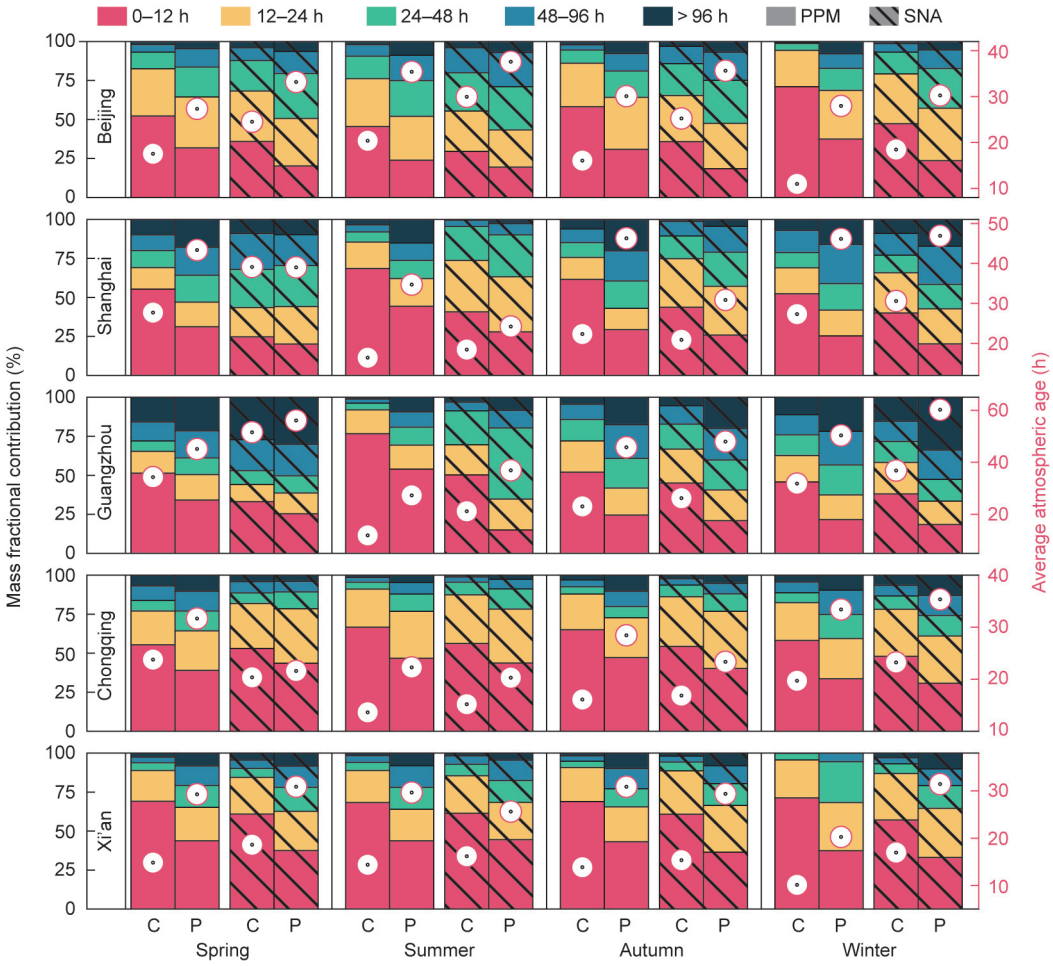

Fig. 8. Comparison of PPM and SNA age distribution on clean days (C; < 75 μg·m^{-3}) and polluted days (P; ≥ 75 μg·m^{-3}) in Beijing, Shanghai, Guangzhou, Chongqing, and Xi'an. The red circle with a black dot indicates the average atmospheric age (in hours, right *y*-axis).

up to 55 μg·m^{-3} on January 24. Aged sulfate particles with atmospheric age > 48 h contribute almost half of the total sulfate in the entire month. On the peak value days, January 23–24, their contributions can reach up to 66%. Such high fractions of aged sulfate particles are mainly attributed to the regional transport of central China and NCP emissions under the prevailing northwesterly wind in winter [34,69]. In July, most sulfate particles are from the first two age bins (0–12 and 12–24 h) because of the enhanced chemical conversion rate and adequate ventilation in summer. However, a large contribution (> 45%) of aged sulfate particles (> 48 h) can occasionally be observed on clean days (July 12–14). For nitrate, the age distribution shows significant day-to-day variations in January. For example, as nitrate concentrations increase, the contributions of the 0–12 and 12–24 h age bins rapidly decrease from 97% on January 20 to 40% on January 21. In July, nitrate concentrations are significantly lower, with concentrations less than 1 μg·m^{-3} on most days. More than 90% of nitrate particles show an atmospheric age of less than 24 h. Ammonium concentrations are predicted to be as high as 20 μg·m^{-3} on January 23–24, but less than 6 μg·m^{-3} throughout July. On clean days, most ammonium particles show an atmospheric age of less than 24 h, while they tend to shift towards old age bins on high concentration days.

4. Discussion

Our study is subject to several uncertainties and limitations. First, the age distribution of the SOA was not considered in the current model framework. SOA constitutes 15%–30% of the $PM_{2.5}$ mass concentration during haze episodes in China [8,25]. However, current models substantially underestimate SOA mass concentrations because of a lack of knowledge regarding its sources, composition, and formation mechanisms [53]. Second, uncertainties in the simulated aerosol mass concentrations may affect the derived aerosol age distribution. Although the predicted $PM_{2.5}$ is consistent with observations, SNA is overestimated by 16.6%–42.8% in China, especially nitrate (Fig. 3). Model biases are likely attributed to the uncertainties associated with emissions, meteorology, grid resolution, and model treatment, which have been extensively discussed in our previous study [30]. Third, the discrete age distribution representation can only calculate the age distribution for limited periods. In other words, only the species older than the highest age that can be explicitly represented are assigned to the final age bin. In addition, according to Eq. (2), the average atmospheric age of pollutants in each age bin was assumed to be equal to the middle of the corresponding period. This assumption can introduce uncertainties in the estimated average atmospheric age because particle concentrations change rapidly with atmospheric age. To address this issue, an additional simulation with an age bin advancing frequency setting of 6 h was conducted in January 2013. As shown in Fig. S14 in Appendix A, the estimated average atmospheric age in Beijing from simulations with a 6-hour age bin advancing interval is lower (4.6–9.4 h) than that from simulations with a 12-hour age bin advancing interval, although the overall temporal variation is consistent.

Despite these uncertainties, the time information of emission sources provided by our age-resolved CMAQ model can help poli-

cymakers design effective emission control strategies in different regions and seasons, especially emergency response measures for large public events such as sports games, parades, and international conferences. Our results suggest that local emission control of PPM could be effective within 12 h for regions with high anthropogenic emissions such as NCP, SCB, and YRD. However, it should be put in force one to two days ahead in winter and spring for southern China such as PRD and southeastern coastal provinces. Sulfate is significantly more aged than PPM and can be transported over a longer distance, indicating that regional transport contributes a large fraction to the rapid growth of sulfate. In winter, regional joint controls of SO_2 emissions are suggested to be put in force at least one to two days ahead in NCP and NE; it should be two to three days in advance in southern China due to the older atmospheric age of sulfate. In summer, controlling the emissions of SO_2 should be put in force one to two days ahead in most parts of China. The formation of nitrate and ammonium involves complex multiphase chemistry, thus, controlling the emissions of their precursor gases NO_x and NH_3 must be considered carefully [70]. In eastern China in winter, a typical NO_x-saturated regime, cutting NO_x emissions could lead to a substantial increase in O_3 and NO_3 radicals, which in turn enhances the formation of secondary $PM_{2.5}$ [71]. Reducing particulate nitrate requires a very deep reduction in NO_x emissions within two days, which can be challenging [71,72]. In contrast, O_3 formation sensitivity in most urban cities shifts to either transition or NO_x-limited regimes in summer [73]. Thus, reducing NO_x emissions within a day is effective for mitigating both nitrate and ammonium formation. Local and regional emission control of NH_3 is suggested to be put in force one to two days ahead in winter and within a day in summer. In addition, the reduction intensity of NH_3 is highly sensitive to ambient NH_3 concentrations. In southern China such as the PRD, the formation of nitrate and ammonium is sensitive to NH_3 reduction because of relatively low NH_3 emission [74]. However, in NH_3-rich regions, such as the NCP and YRD, a large NH_3 emission reduction is required. Studies indicate that cutting NH_3 emissions by 20%–40% only leads to a 1.4–3.8 $\mu g \cdot m^{-3}$ reduction of $PM_{2.5}$ but a 60%–100% reduction of NH_3 emission could decrease $PM_{2.5}$ by 8.1–26.7 $\mu g \cdot m^{-3}$ [75]. Nonetheless, controlling NH_3 emissions can be much more effective on haze days, because of the rapidly increasing particulate nitrate concentrations [65].

5. Conclusions

In this study, the age-resolved CMAQ model was applied to estimate the age distribution of the primary and secondary $PM_{2.5}$ components over China in the entire year of 2013. Compared with ground-based observations, the model can reasonably capture the spatial and temporal variations of $PM_{2.5}$, sulfate, nitrate, and ammonium. High concentrations of fresh PPM and ammonium with atmospheric age < 24 h are observed in source regions such as the NCP and YRD, indicating a large contribution from local emissions. Sulfate is considerably more aged than PPM. The concentrations of sulfate particles with atmospheric age > 96 h reach up to 15 $\mu g \cdot m^{-3}$ in the SCB during winter. The age distribution of PPM, ammonium, and sulfate show large seasonal variations in the YRD, PRD, and SCB, with a higher average age in winter and lower in summer. In contrast, small seasonal variations (< 6.5 h) occur in the NCP and FWP, with an average age of approximately 20–30 h for PPM and ammonium, and 40–56 h for sulfate. Nitrate is more concentrated in the 12–24 h age bin, and its age distribution shows a dramatic seasonal variation. The average age in winter is about 35–50 h for eastern China, which is significantly higher than that in summer (~18–30 h). In addition, the contribution of old age bins (> 24 h) increases remarkably during pollution days in most cities and seasons for all the species, especially on the peak value days, suggesting that regional transport plays an important role during severe haze events. The age distribution of air pollutants provided in this study can provide valuable time information on $PM_{2.5}$ emission sources, which can help policymakers design timely control measures to effectively reduce $PM_{2.5}$ levels in different regions and seasons.

Acknowledgments

This work was supported by the National Key Research and Development (R&D) Program of China (2019YFA0606802), the National Natural Science Foundation of China (41975162 and 42021004), and the Jiangsu Environmental Protection Research Project (2016015).

Compliance with ethics guidelines

Xiaodong Xie, Qi Ying, Hongliang Zhang, and Jianlin Hu declare that they have no conflict of interest or financial conflicts to disclose.

Appendix A. Supplementary data

Supplementary data to this article can be found online at https://doi.org/10.1016/j.eng.2022.03.013.

References

[1] Cohen AJ, Brauer M, Burnett R, Anderson HR, Frostad J, Estep K, et al. Estimates and 25-year trends of the global burden of disease attributable to ambient air pollution: an analysis of data from the Global Burden of Diseases Study 2015. Lancet 2017;389(10082):1907–18.
[2] The Intergovernmental Panel on Climate Change (IPCC). Climate change 2021: the physical science basis. Contribution of Working Group I to the Sixth Assessment Report of the Intergovernmental Panel on Climate Change. Cambridge, UK and New York, NY, USA: Cambridge University Press; 2021.
[3] Riemer N, Ault AP, West M, Craig RL, Curtis JH. Aerosol mixing state: measurements, modeling, and impacts. Rev Geophys 2019;57(2):187–249.
[4] Wagstrom KM, Pandis SN. Determination of the age distribution of primary and secondary aerosol species using a chemical transport model. J Geophys Res Atmos 2009;114(D14):D14303.
[5] Huang RJ, Zhang Y, Bozzetti C, Ho KF, Cao JJ, Han Y, et al. High secondary aerosol contribution to particulate pollution during haze events in China. Nature 2014;514(7521):218–22.
[6] Xie Y, Dai H, Dong H, Hanaoka T, Masui T. Economic impacts from $PM_{2.5}$ pollution-related health effects in China: a provincial-level analysis. Environ Sci Technol 2016;50(9):4836–43.
[7] Zhang Q, Zheng Y, Tong D, Shao M, Wang S, Zhang Y, et al. Drivers of improved $PM_{2.5}$ air quality in China from 2013 to 2017. Proc Natl Acad Sci USA 2019;116(49):24463–9.
[8] Li YJ, Sun Y, Zhang Q, Li X, Li M, Zhou Z, et al. Real-time chemical characterization of atmospheric particulate matter in China: a review. Atmos Environ 2017;158:270–304.
[9] An Z, Huang RJ, Zhang R, Tie X, Li G, Cao J, et al. Severe haze in northern China: a synergy of anthropogenic emissions and atmospheric processes. Proc Natl Acad Sci USA 2019;116(18):8657–66.
[10] Hu J, Wu L, Zheng B, Zhang Q, He K, Chang Q, et al. Source contributions and regional transport of primary particulate matter in China. Environ Pollut 2015;207:31–42.
[11] Zhu Y, Huang L, Li J, Ying Q, Zhang H, Liu X, et al. Sources of particulate matter in China: insights from source apportionment studies published in 1987–2017. Environ Int 2018;115:343–57.
[12] Li L, Hu J, Li J, Gong K, Wang X, Ying Q, et al. Modelling air quality during the EXPLORE-YRD campaign—part II. Regional source apportionment of ozone and $PM_{2.5}$. Atmos Environ 2021;247:118063.
[13] Shi Z, Li J, Huang L, Wang P, Wu L, Ying Q, et al. Source apportionment of fine particulate matter in China in 2013 using a source-oriented chemical transport model. Sci Total Environ 2017;601–602:1476–87.
[14] Gong K, Li L, Li J, Qin M, Wang X, Ying Q, et al. Quantifying the impacts of intercity transport on air quality in the Yangtze River Delta urban agglomeration, China: implications for regional cooperative controls of $PM_{2.5}$ and O_3. Sci Total Environ 2021;779:146619.
[15] Wu JB, Wang Z, Wang Q, Li J, Xu J, Chen H, et al. Development of an on-line source-tagged model for sulfate, nitrate and ammonium: a modeling study for highly polluted periods in Shanghai. China Environ Pollut 2017;221:168–79.
[16] Roberts JM, Fehsenfeld FC, Liu SC, Bollinger MJ, Hahn C, Albritton DL, et al. Measurements of aromatic hydrocarbon ratios and NO_x concentrations in the

rural troposphere: observation of air mass photochemical aging and NO_x removal. Atmos Environ 1984;18(11):2421–32.
[17] Parrish DD, Hahn CJ, Williams EJ, Norton RB, Fehsenfeld FC, Singh HB, et al. Indications of photochemical histories of Pacific air masses from measurements of atmospheric trace species at Point Arena. California J Geophys Res Atmos 1992;97(D14):15883–901.
[18] Irei S, Takami A, Sadanaga Y, Nozoe S, Yonemura S, Bandow H, et al. Photochemical age of air pollutants, ozone, and secondary organic aerosol in transboundary air observed on Fukue Island, Nagasaki. Japan Atmos Chem Phys 2016;16(7):4555–68.
[19] Kleinman LI, Daum PH, Lee YN, Nunnermacker LJ, Springston SR, Weinstein-Lloyd J, et al. Photochemical age determinations in the Phoenix metropolitan area. J Geophys Res Atmos 2003;108(D3):4096.
[20] Doran JC, Fast JD, Barnard JC, Laskin A, Desyaterik Y, Gilles MK. Applications of lagrangian dispersion modeling to the analysis of changes in the specific absorption of elemental carbon. Atmos Chem Phys 2008;8(5):1377–89.
[21] Parrish DD, Stohl A, Forster C, Atlas EL, Blake DR, Goldan PD, et al. Effects of mixing on evolution of hydrocarbon ratios in the troposphere. J Geophys Res Atmos 2007;112(D10):D10S34.
[22] Han Q, Zender CS. Desert dust aerosol age characterized by mass-age tracking of tracers. J Geophys Res Atmos 2010;115(D22):D22201.
[23] Ying Q, Zhang J, Zhang H, Hu J, Kleeman MJ. Atmospheric age distribution of primary and secondary inorganic aerosols in a polluted atmosphere. Environ Sci Technol 2021;55(9):5668–76.
[24] Xie X, Shi Z, Ying Q, Zhang H, Hu J. Age-resolved source and region contributions to fine particulate matter during an extreme haze episode in China. Geophys Res Lett 2021;48(21): e2021GL095388.
[25] Chen Q, Fu TM, Hu J, Ying Q, Zhang L. Modelling secondary organic aerosols in China. Natl Sci Rev 2017;4(6):806–9.
[26] Byun DW, Ching JKS. Science algorithms of the EPA Models-3 Community Multiscale Air Quality (CMAQ) modeling system. Washington, DC: US Environmental Protection Agency. 1999 Jun 29. Report No.: EPA/600/R-99/030 (NTIS PB2000-100561).
[27] Guo H, Kota SH, Sahu SK, Hu J, Ying Q, Gao A, et al. Source apportionment of $PM_{2.5}$ in North India using source-oriented air quality models. Environ Pollut 2017;231(Pt 1):426–36.
[28] Wang J, Xing J, Mathur R, Pleim JE, Wang S, Hogrefe C, et al. Historical trends in $PM_{2.5}$-related premature mortality during 1990–2010 across the Northern Hemisphere. Environ Health Perspect 2017;125(3):400–8.
[29] Hogrefe C, Liu P, Pouliot G, Mathur R, Roselle S, Flemming J, et al. Impacts of different characterizations of large-scale background on simulated regional-scale ozone over the continental United States. Atmos Chem Phys 2018;18(5):3839–64.
[30] Hu J, Chen J, Ying Q, Zhang H. One-year simulation of ozone and particulate matter in China using WRF/CMAQ modeling system. Atmos Chem Phys 2016;16(16):10333–50.
[31] Wang LT, Wei Z, Yang J, Zhang Y, Zhang FF, Su J, et al. The 2013 severe haze over southern Hebei, China: model evaluation, source apportionment, and policy implications. Atmos Chem Phys 2014;14(6):3151–73.
[32] Cheng J, Su J, Cui T, Li X, Dong X, Sun F, et al. Dominant role of emission reduction in $PM_{2.5}$ air quality improvement in Beijing during 2013–2017: a model-based decomposition analysis. Atmos Chem Phys 2019;19(9):6125–46.
[33] Wang C, Wang Y, Shi Z, Sun J, Gong K, Li J, et al. Effects of using different exposure data to estimate changes in premature mortality attributable to $PM_{2.5}$ and O_3 in China. Environ Pollut 2021;285:117242.
[34] Ying Q, Wu L, Zhang H. Local and inter-regional contributions to $PM_{2.5}$ nitrate and sulfate in China. Atmos Environ 2014;94:582–92.
[35] Qiao X, Ying Q, Li X, Zhang H, Hu J, Tang Y, et al. Source apportionment of $PM_{2.5}$ for 25 Chinese provincial capitals and municipalities using a source-oriented Community Multiscale Air Quality model. Sci Total Environ 2018;612:462–71.
[36] Ying Q, Li J, Kota SH. Significant contributions of isoprene to summertime secondary organic aerosol in eastern United States. Environ Sci Technol 2015;49(13):7834–72.
[37] Hu J, Wang P, Ying Q, Zhang H, Chen J, Ge X, et al. Modeling biogenic and anthropogenic secondary organic aerosol in China. Atmos Chem Phys 2017;17(1):77–92.
[38] Li J, Zhang H, Ying Q, Wu Z, Zhang Y, Wang X, et al. Impacts of water partitioning and polarity of organic compounds on secondary organic aerosol over eastern China. Atmos Chem Phys 2020;20(12):7291–306.
[39] Zhang H, Li J, Ying Q, Yu JZ, Wu D, Cheng Y, et al. Source apportionment of $PM_{2.5}$ nitrate and sulfate in China using a source-oriented chemical transport model. Atmos Environ 2012;62:228–42.
[40] Zheng B, Tong D, Li M, Liu F, Hong C, Geng G, et al. Trends in China's anthropogenic emissions since 2010 as the consequence of clean air actions. Atmos Chem Phys 2018;18(19):14095–111.
[41] Kurokawa J, Ohara T. Long-term historical trends in air pollutant emissions in Asia: regional emission inventory in Asia (REAS) version 3. Atmos Chem Phys 2020;20(21):12761–93.
[42] Guenther A, Karl T, Harley P, Wiedinmyer C, Palmer PI, Geron C. Estimates of global terrestrial isoprene emissions using MEGAN (Model of Emissions of Gases and Aerosols from Nature). Atmos Chem Phys 2006;6(11):3181–210.
[43] Wiedinmyer C, Akagi SK, Yokelson RJ, Emmons LK, Al-Saadi JA, Orlando JJ, et al. The Fire INventory from NCAR (FINN): a high resolution global model to estimate the emissions from open burning. Geosci Model Dev 2011;4(3):625–41.
[44] Zhang H, Guo H, Hu J, Ying Q, Kleeman MJ. Modeling Atmospheric age distribution of elemental carbon using a regional age-resolved particle representation framework. Environ Sci Technol 2019;53(1):270–8.
[45] Zhai S, Jacob DJ, Wang X, Liu Z, Wen T, Shah V, et al. Control of particulate nitrate air pollution in China. Nat Geosci 2021;14(6):389–95.
[46] Liu Z, Gao W, Yu Y, Hu B, Xin J, Sun Y, et al. Characteristics of $PM_{2.5}$ mass concentrations and chemical species in urban and background areas of China: emerging results from the CARE-China network. Atmos Chem Phys 2018;18(12):8849–71.
[47] Xin J, Wang Y, Pan Y, Ji D, Liu Z, Wen T, et al. The campaign on atmospheric aerosol research network of China: CARE-China. Bull Am Meteorol Soc 2015;96(7):1137–55.
[48] Emery C, Liu Z, Russell AG, Odman MT, Yarwood G, Kumar N. Recommendations on statistics and benchmarks to assess photochemical model performance. J Air Waste Manag Assoc 2017;67(5):582–98.
[49] Emery C, Tai E, Yarwood G. Enhanced meteorological modeling and performance evaluation for two texas ozone episodes. Report. Novato, CA: Environmental International Corporation; 2001.
[50] Wang P, Cao JJ, Shen ZX, Han YM, Lee SC, Huang Y, et al. Spatial and seasonal variations of $PM_{2.5}$ mass and species during 2010 in Xi'an, China. Sci Total Environ 2015;508:477–87.
[51] Sun YL, Wang ZF, Du W, Zhang Q, Wang QQ, Fu PQ, et al. Long-term real-time measurements of aerosol particle composition in Beijing, China: seasonal variations, meteorological effects, and source analysis. Atmos Chem Phys 2015;15(17):10149–65.
[52] Qiao X, Guo H, Wang P, Tang Y, Ying Q, Zhao X, et al. Fine particulate matter and ozone pollution in the 18 cities of the Sichuan Basin in southwestern China: model performance and characteristics. Aerosol Air Qual Res 2019;19(10):2308–19.
[53] Hallquist M, Wenger JC, Baltensperger U, Rudich Y, Simpson D, Claeys M, et al. The formation, properties and impact of secondary organic aerosol: current and emerging issues. Atmos Chem Phys 2009;9(14):5155–236.
[54] Chen X, Wang Z, Yu F, Pan X, Li J, Ge B, et al. Estimation of atmospheric aging time of black carbon particles in the polluted atmosphere over central–eastern China using microphysical process analysis in regional chemical transport model. Atmos Environ 2017;163:44–56.
[55] Huang K, Fu JS, Hsu NC, Gao Y, Dong X, Tsay SC, et al. Impact assessment of biomass burning on air quality in Southeast and East Asia during BASE-ASIA. Atmos Environ 2013;78:291–302.
[56] Long X, Tie X, Cao J, Huang R, Feng T, Li N, et al. Impact of crop field burning and mountains on heavy haze in the North China Plain: a case study. Atmos Chem Phys 2016;16(15):9675–91.
[57] Li M, Zhang Q, Kurokawa JI, Woo JH, He K, Lu Z, et al. MIX: a mosaic Asian anthropogenic emission inventory under the international collaboration framework of the MICS-Asia and HTAP. Atmos Chem Phys 2017;17(2):935–63.
[58] Zheng GJ, Duan FK, Su H, Ma YL, Cheng Y, Zheng B, et al. Exploring the severe winter haze in Beijing: the impact of synoptic weather, regional transport and heterogeneous reactions. Atmos Chem Phys 2015;15(6):2969–83.
[59] Zhu J, Wang S, Wang H, Jing S, Lou S, Saiz-Lopez A, et al. Observationally constrained modeling of atmospheric oxidation capacity and photochemical reactivity in Shanghai, China. Atmos Chem Phys 2020;20(3):1217–32.
[60] Ji D, Gao W, Zhang J, Morino Y, Zhou L, Yu P, et al. Investigating the evolution of summertime secondary atmospheric pollutants in urban Beijing. Sci Total Environ 2016;572:289–300.
[61] Lee C, Martin RV, van Donkelaar A, Lee H, Dickerson RR, Hains JC, et al. SO_2 emissions and lifetimes: estimates from inverse modeling using *in situ* and global, space-based (SCIAMACHY and OMI) observations. J Geophys Res Atmos 2011;116(D6):D06304.
[62] Shah V, Jacob DJ, Li K, Silvern RF, Zhai S, Liu M, et al. Effect of changing NO_x lifetime on the seasonality and long-term trends of satellite-observed tropospheric NO_2 columns over China. Atmos Chem Phys 2020;20(3):1483–95.
[63] Fischer EV, Jacob DJ, Yantosca RM, Sulprizio MP, Millet DB, Mao J, et al. Atmospheric peroxyacetyl nitrate (PAN): a global budget and source attribution. Atmos Chem Phys 2014;14(5):2679–98.
[64] Pinder RW, Dennis RL, Bhave PV. Observable indicators of the sensitivity of $PM_{2.5}$ nitrate to emission reductions—part I: derivation of the adjusted gas ratio and applicability at regulatory-relevant time scales. Atmos Environ 2008;42(6):1275–86.
[65] Liu M, Huang X, Song Y, Tang J, Cao J, Zhang X, et al. Ammonia emission control in China would mitigate haze pollution and nitrogen deposition, but worsen acid rain. Proc Natl Acad Sci USA 2019;116(16):7760–5.
[66] Leung DM, Shi H, Zhao B, Wang J, Ding EM, Gu Y, et al. Wintertime particulate matter decrease buffered by unfavorable chemical processes despite emissions reductions in China. Geophys Res Lett 2020;47(14): e2020GL087721.
[67] Nenes A, Pandis SN, Kanakidou M, Russell AG, Song S, Vasilakos P, et al. Aerosol acidity and liquid water content regulate the dry deposition of inorganic reactive nitrogen. Atmos Chem Phys 2021;21(8):6023–33.
[68] Dammers E, McLinden CA, Griffin D, Shephard MW, Van Der Graaf S, Lutsch E, et al. NH_3 emissions from large point sources derived from CrIS and IASI satellite observations. Atmos Chem Phys 2019;19(19):12261–93.
[69] Huang X, Ding A, Wang Z, Ding K, Gao J, Chai F, et al. Amplified transboundary transport of haze by aerosol–boundary layer interaction in China. Nat Geosci 2020;13(6):428–34.

[70] Lim YB, Seo J, Kim JY, Kim YP, Jin HC. Local formation of sulfates contributes to the urban haze with regional transport origin. Environ Res Lett 2020;15(8):084034.
[71] Huang X, Ding A, Gao J, Zheng B, Zhou D, Qi X, et al. Enhanced secondary pollution offset reduction of primary emissions during COVID-19 lockdown in China. Natl Sci Rev 2020;8(2):nwaa137.
[72] Li M, Zhang Z, Yao Q, Wang T, Xie M, Li S, et al. Nonlinear responses of particulate nitrate to NO_x emission controls in the megalopolises of China. Atmos Chem Phys 2021;21(19):15135–52.
[73] Kang M, Zhang J, Zhang H, Ying Q. On the relevancy of observed ozone increase during COVID-19 lockdown to summertime ozone and $PM_{2.5}$ control policies in China. Environ Sci Technol Lett 2021;8(4):289–94.
[74] Wang S, Xing J, Jang C, Zhu Y, Fu JS, Hao J. Impact assessment of ammonia emissions on inorganic aerosols in East China using response surface modeling technique. Environ Sci Technol 2011;45(21):9293–300.
[75] Liu Z, Zhou M, Chen Y, Chen D, Pan Y, Song T, et al. The nonlinear response of fine particulate matter pollution to ammonia emission reductions in north China. Environ Res Lett 2021;16:034014.